ADVANCED FUNCTIONAL MATERIALS
www.afm-journal.de

Benzimidazole Based Hole-Transporting Materials for High-performance Inverted Perovskite Solar Cells

Yogesh S. Tingare, Chaochin Su,* Ja-Hon Lin, Yi-Chun Hsieh, Hong-Jia Lin, Ya-Chun Hsu, Meng-Che Li, Guan-Lin Chen, Kai-Wei Tseng, Yi-Hsuan Yang, Leeyih Wang, Hsinhan Tsai,* Wanyi Nie,* and Wen-Ren Li**

Interfaces play a decisive role in perovskite solar cells' power conversion efficiency and their long-term durability. Small-molecule hole-transporting materials (HTMs) have grabbed enormous attention due to their structural flexibility, material properties, and stabilities, allowing for improved operational durability in perovskite photovoltaics. This study synthesizes and investigates a new class of benzimidazole-based small molecules, named YJS001 and YJS003, serving as the HTMs to enable high-efficiency mixed-cation mixed-halide perovskite solar cells. The benzimidazole-based materials are dopant-free HTMs composed of donor and acceptor building blocks that are designed to engineer the energy level alignment near the HTM/perovskite interface. Mixed-cation mixed-halide perovskites can be grown uniformly on both HTMs with large crystalline grains. It is discovered that the donor-rich YJS003-based solar cell exhibits a high open-circuit voltage of 1.09 V with a champion power conversion efficiency of over 20%. Power-dependent current–voltage characteristics of the solar cells are analyzed, from which the high performance of YJS003's excellent hole mobility and well-aligned energy level is attributed. This work introduces a new class of benzimidazole-based small molecules as HTMs, that paves the path for dopant free interface material development for commercialization of perovskite solar cells.

1. Introduction

Halide perovskite solar cells (PSCs) are recent champion technologies for solar energy conversion to electricity and fuels. The devices can be manufactured at a low-cost from a solution yielding high power conversion efficiencies (PCEs) over 25%,[1] which open a new gateway for utilizing renewable energy.[2] In the past decade, PSC research has progressed significantly with a rapid boost in power conversion efficiency, positioning them on par with other photovoltaic candidates such as silicon and CdTe solar cells.[3] There are mainly two types of architectures of PSCs: regular (*n-i-p*) and inverted (*p-i-n*), where the latter holds an upper hand to simplify the device fabrication process.[4]

Among the various components that comprise the device assembly, the perovskite layers and hole-transporting materials (HTM) have been extensively optimized to achieve high-performing PSCs.[5] The crystallinity and mixed-cation mixed-halide composition of the perovskite layer significantly impact the PSC's overall efficiency.[6] In addition, the use of differently configured perovskites can alter the absorber film's bandgap, thereby facilitating electron transfer.[7] The second crucial component that benefits the efficiency of PSCs is the HTM layer.[8] HTMs play important roles in efficiently extracting and transporting positive charges and reducing carriers recombination in PSCs.[9] It

Y. S. Tingare, C. Su, H.-J. Lin, Y.-C. Hsu, M.-C. Li
Institute of Organic and Polymeric Materials/Research and Development Center for Smart Textile Technology
National Taipei University of Technology
Taipei 106344, Taiwan
E-mail: f12098@ntut.edu.tw; f10913@mail.ntut.edu.tw

J.-H. Lin
Department of Electro-Optical Engineering
National Taipei University of Technology
Taipei 106344, Taiwan

The ORCID identification number(s) for the author(s) of this article can be found under https://doi.org/10.1002/adfm.202201933.

© 2022 National Central University/National Taipei University of Technology. Advanced Functional Materials published by Wiley-VCH GmbH. This is an open access article under the terms of the Creative Commons Attribution License, which permits use, distribution and reproduction in any medium, provided the original work is properly cited.

DOI: 10.1002/adfm.202201933

Y.-C. Hsieh, Y.-H. Yang, W.-R. Li
Department of Chemistry
National Central University
Zhongli 32001, Taiwan
E-mail: ch01@ncu.edu.tw

G.-L. Chen, K.-W. Tseng, L. Wang
Center for Condensed Matter Sciences/Institute of Polymer Science and Engineering/Center of Atomic Initiative for New Materials
National Taiwan University
Taipei 10617, Taiwan

H. Tsai, W. Nie
Center for Integrated Nanotechnologies
Materials Physics and Application Division
Los Alamos National Laboratory
Los Alamos, NM 87545, USA
E-mail: hsinhantsai@lanl.gov; wanyi@lanl.gov

© 2022 National Central University/National Taipei University of Technology. Advanced Functional Materials published by Wiley-VCH GmbH

can also protect the active layer against moisture that improves the operational stability for *n-i-p* PSCs. Because the HTM layer is sandwiched between the transparent electrode and the perovskite film in *p-i-n* PSCs,[3f,10] its properties contribute significantly to PSC performance and must be carefully adjusted. The most commonly used HTM in *p-i-n* PSC is poly(3,4-ethylenedioxythiophene): poly(styrenesulfonate) (**PEDOT:PSS**).[11] However, difficult synthesis and acidic nature as well as the complications in controlling the desired physical properties such as energy levels restrict its use as a potential HTM in PSCs.[12] It is now obvious that introducing HTMs to PSC devices could led to a noteworthy improvement in PCEs. Therefore, developing new HTMs that can offer superior control over their electronic tunability, doping, and solvent compatibility has become one of the top priorities in PSC research.

Small molecule HTMs with various central cores, such as carbazole, xanthene, triazatruxene, fluoranthene, benzothiophene, benzothiadiazole, ethylenedioxythiophene, thienothiophene, ethylrhodanine, malononitrile, diketopyrrolopyrrole, and phenoxazine have been surfaced and found their applications in PSCs.[13] The shape of the molecule (i.e., linear chain, star, or butterfly) can be designed by tuning the organic building blocks, which provides ample space for tuning the conductivity and energy levels.[13c,14] In addition, functional groups like carbonyl, pyridine, sulfur atom-containin, and ionic HTMs can be added in small molecules that can passivate the defects and assist the growth of large grain size perovskites essential for achieving durable performances.[3f,15] Among the reported works, the majority of HTMs have symmetric donor-π-donor (D-π-D) structures with low-lying highest occupied molecular orbital (HOMO) energy levels and impressive hole mobilities. Recently, some molecules containing electron-deficient moieties as acceptors were introduced as HTMs that can drive charge separation in the ground state to promote electron delocalization and subsequently benefit the PSC efficiencies.[3f,16] However, no comparative study between two HTMs with electron donors or deficient moieties in the same structural design has been reported.

In the present work, we design and study **YJS001** and **YJS003** (**Figure 1**a,b) as HTMs with a thiophene-benzimidazole template as the central core. This new class of small-molecule HTMs provides suitable energy levels to the perovskite absorber, and forms π-π stacking to assist the hole transport from the solar cells.[17] As in the HTM/perovskite interface, the hydrogen in the benzimidazole backbone can passivate the defects or stabilize the halides in the perovskite through hydrogen-bonding interaction that further increases the cohesion between the individual perovskite crystal forming on top of the HTM, therefore smoothing its morphology.[18] The bipyridine group at each **YJS001** and **YJS003** HTM terminal is expected to form chelation with metal ions, providing better interfacial interactions between the HTM and perovskite layer.[19] Tuning the central core in HTMs provides choices toward versatility of energy-band engineering and flexibility in structural design. Furthermore, we believe that such adjustment of interlayer band alignment of these thiophene-benzimidazole-based HTMs with the perovskites could provide a higher degree of hole mobility and reduced recombination. Also, good quality perovskite formation and higher PCE performance are predicted for these novel HTMs with the possible intimate interlayer interaction.

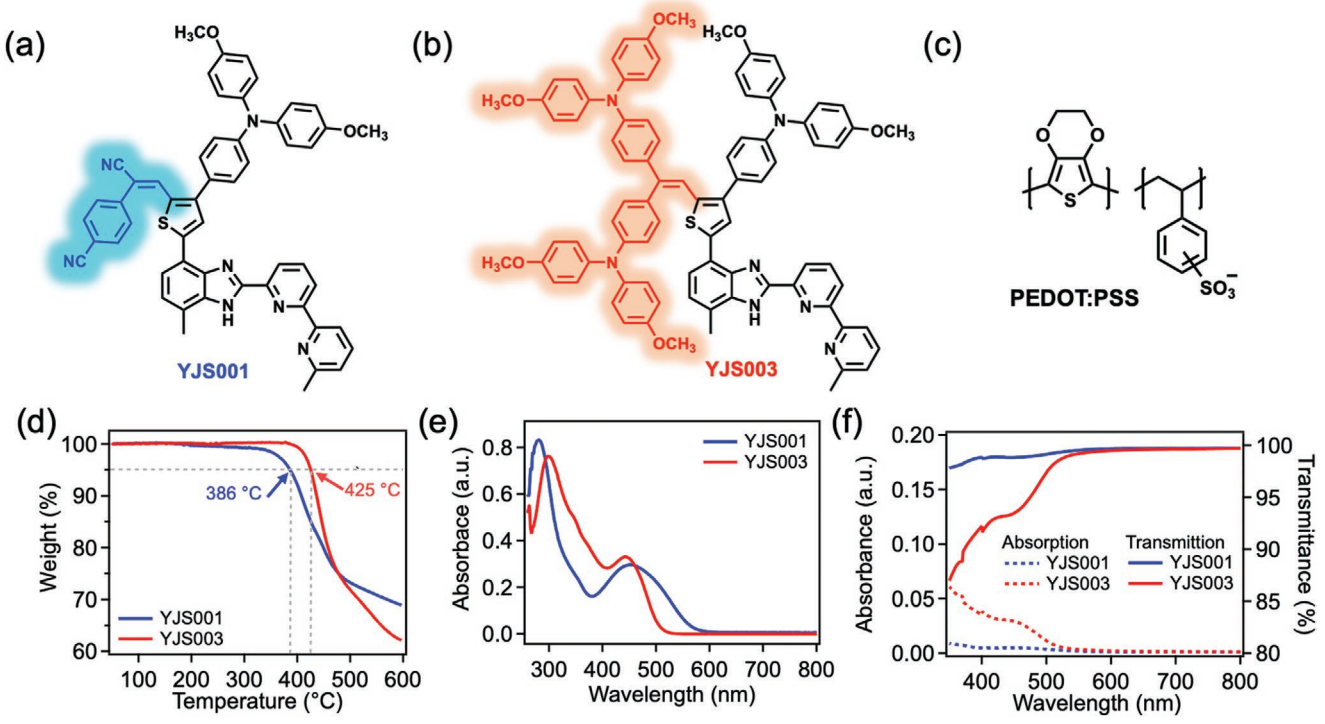

Figure 1. Molecular structures of HTM a) **YJS001**, b) **YJS003**, and c) **PEDOT:PSS**. d) Thermogravimetric analysis graphs of HTM **YJS001** and **YJS003**. e) UV–vis absorption spectra of **YJS001** and **YJS003** in DMF solutions and f) UV-vis transmittance spectra of **YJS001** and **YJS003** films.

© 2022 National Central University/National Taipei University of Technology. Advanced Functional Materials published by Wiley-VCH GmbH

Table 1. Thermal, optical and electrochemical properties of new HTMs.

HTMs	λ_{max} [nm]		λ_{PL} [nm][c)]	$E_g^{optd)}$ [eV]	E_{HOMO} [eV]	E_{LUMO}[e)] [eV]	T_d [°C]
	Solution[a)]	Film[b)]					
YJS001	281, 452	450	770	2.27	−5.40	−3.13	386
YJS003	298, 442	439	773	2.45	−5.24	−2.79	425

[a)]Absorption spectra in DMF solutions; [b)]Absorption spectra on films; [c)]Emission spectra analysed in solutions; [d)]Calculated optical bandgap using the formula 1240/λ onset; [e)]$E_{LUMO} = E_{HOMO} + E_g^{opt}$.

In HTM **YJS001**, the thiophene-benzimidazole back-bone that acts as a template is substituted with 4-cyanobenzeneacetonitrile as the acceptor moiety and 4,4′-dimethoxytriphenylamine (OMeTPA) as a donor unit (Figure 1a). An excellent HTMs required appropriate HOMO/lowest unoccupied molecular orbital (LUMO) energy levels that match the perovskite's energy band alignment, which can facilitate hole transport and prevent electron recombination with improved open-circuit voltage (V_{OC}). We first probe the HOMO and the LUMO of **YJS001** are at −5.40 and −3.13 eV (**Table 1**), respectively, derived from cyclic voltammetry (Figure S1, Supporting Information) and UV-Vis absorption curves. Changing the 4-cyanobenzeneacetonitrile acceptor in **YJS001** to a donor unit in **YJS003** (Figure 1b) lifted the HOMO and LUMO energy levels to −5.24 (0.16 eV lower) and −2.79 eV (0.34 eV higher), respectively, shown in Table 1, thus a better hole extraction and electron blocking capability is expected from the **YJS003** HTM. These results show that energy level engineering can be manipulated and governed by systematic design the molecular modification of donor/acceptor substituents in HTMs.

2. Results and Discussion

The detailed synthetic routes (Scheme S1 and S2, Supporting Information) and reaction conditions for **YJS001** and **YJS003** can be found in the experimental section of Supporting Information. The thermal properties of **YJS001** and **YJS003** (Figure 1d) were tested via thermogravimetric analysis (TGA). The decomposition temperatures (T_d) (at 5% weight loss) of HTM **YJS001** (386 °C) and **YJS003** (425 °C) are sufficiently high, indicating that both HTMs are thermally stable. The optical properties of the two new HTMs, **YJS001** and **YJS003**, in solutions, were investigated using UV-Vis absorption spectroscopy and shown in Figure 1e, while the relevant parameters are shown in Table 1. Also, the UV–vis absorption and transmittance of **YJS001** and **YJS003** films were recorded, and their spectra are displayed in Figure 1f. The absorption spectra of both **YJS001** and **YJS003** in solutions showed a strong peak at 281 and 298 nm, respectively, corresponding to the π–π^* local electron transition of the TPA units. The weaker peak in **YJS001** at 452 nm is attributed to the π–π^* electron transition between the benzimidazole core and the acceptor moiety and partly from the bipyridyl unit of **YJS001**. In the case of **YJS003**, the corresponding peak with slightly higher intensity appears at 442 nm and is blue-shifted due to replacing the acceptor with the donor moiety. Meanwhile, the UV absorption spectra of **YJS001** and **YJS003** thin films also showed similar phenomena in solutions. The absorption maximum of **YJS001** on film appeared at 450 nm, while **YJS003** showed at 439 nm. Compared to those in solutions, the slightly blue-shifted and broad UV absorption on films indicates intermolecular interactions in the solid-state (Figure S2, Supporting Information). For HTM to be efficient in the *p-i-n* architecture PSC, it should have optical transparency in the range between 450–850 nm so that the perovskite layer coated on its top can have good light harvesting. Both **YJS001** and **YJS003** display a similar transmittance range between 500–900 nm. The optimal value of transmittance obtained for HTM **YJS001** and **YJS003** are 515 nm and 550 nm, respectively.

Before device fabrication, it is important to understand the quality of the perovskite layer coated on the HTMs. This study utilizes a $Cs_{0.05}FA_{0.78}MA_{0.17}PbI_{2.53}Br_{0.47}$ triple-cation lead mixed-halide perovskite composition prepared in a single step. We use a scanning electron microscope (SEM) to characterize the perovskite thin-film morphology and uniformity, X-ray diffration (XRD) is employed for crystal structure characterization, and electronic properties are probed by optical spectroscopy and current–voltage measurements. These results are summarized in **Figure 2**. Figure 2a,b shows the surface SEM images of perovskite thin films deposited on **YJS001** and **YJS003** HTMs, respectively. Both SEM images indicate that flat and uniform perovskite layer could be produced on both HTMs. This is possibly due to the hydrophobicity difference from these HTMs. Therefore, we performed contact angle experiments on these HTMs. The contact angle (θ) data of the **YJS001** layer showed the θ with 45.54° (Figure 2a inset). Compared to the **YJS003** layer, the contact angle value is much higher (θ = 67.07°) (Figure 2b inset), implying the lower wetting capability on the surface. This result is consistent with previous reports that a non-wetting surface can facilitate crystal growth.[20] The contact angle of **PEDOT:PSS** layer is much lower (15.14° θ) (Figure S3, Supporting Information) than that of **YJS001** and **YJS003**. We further assembled the devices and imaged the cross-sectional views for these devices with **YJS001** and **YJS003**. Figure 2c,d shows that both perovskite layers on **YJS001** and **YJS003** are compact and homogenous with uniform coverage over a large area. The average perovskite film thickness is 608 ± 2.43 nm for **YJS001** devices and 616 ± 2.89 nm for **YJS003** devices, which are comparable. However, the grain size from the cross-sectional view differs in the two samples. In the **YJS001** device, the perovskite film consists of multiple crystals with grain sizes between 270 and 460 nm, whereas the **YJS003** device has fewer and larger crystals between 730 and 995 nm. The above results match the surface SEM observation and imply that the perovskite thin film on **YJS003** has less grain boundary with reduced defect sites.

To further characterize the crystal structures, we performed XRD on perovskite thin films (Figure 2e) and extracted the full width at half maximum (FWHM) of the dominant peaks (Figure 2f). From XRD patterns, the dominant planes are (110), (112), (220), and (213) corresponding to the tetragonal phase perovskites which match with previous reports elsewhere.[21] When we extract the FWHM of these dominant planes from XRD data (Figure 2f), the FHWM of **PEDOT:PESS** is much larger than **YJS001** and **YJS003**. Besides, the **YJS003** has the smallest FWHM representing the best crystallinity, which

© 2022 National Central University/National Taipei University of Technology. Advanced Functional Materials published by Wiley-VCH GmbH

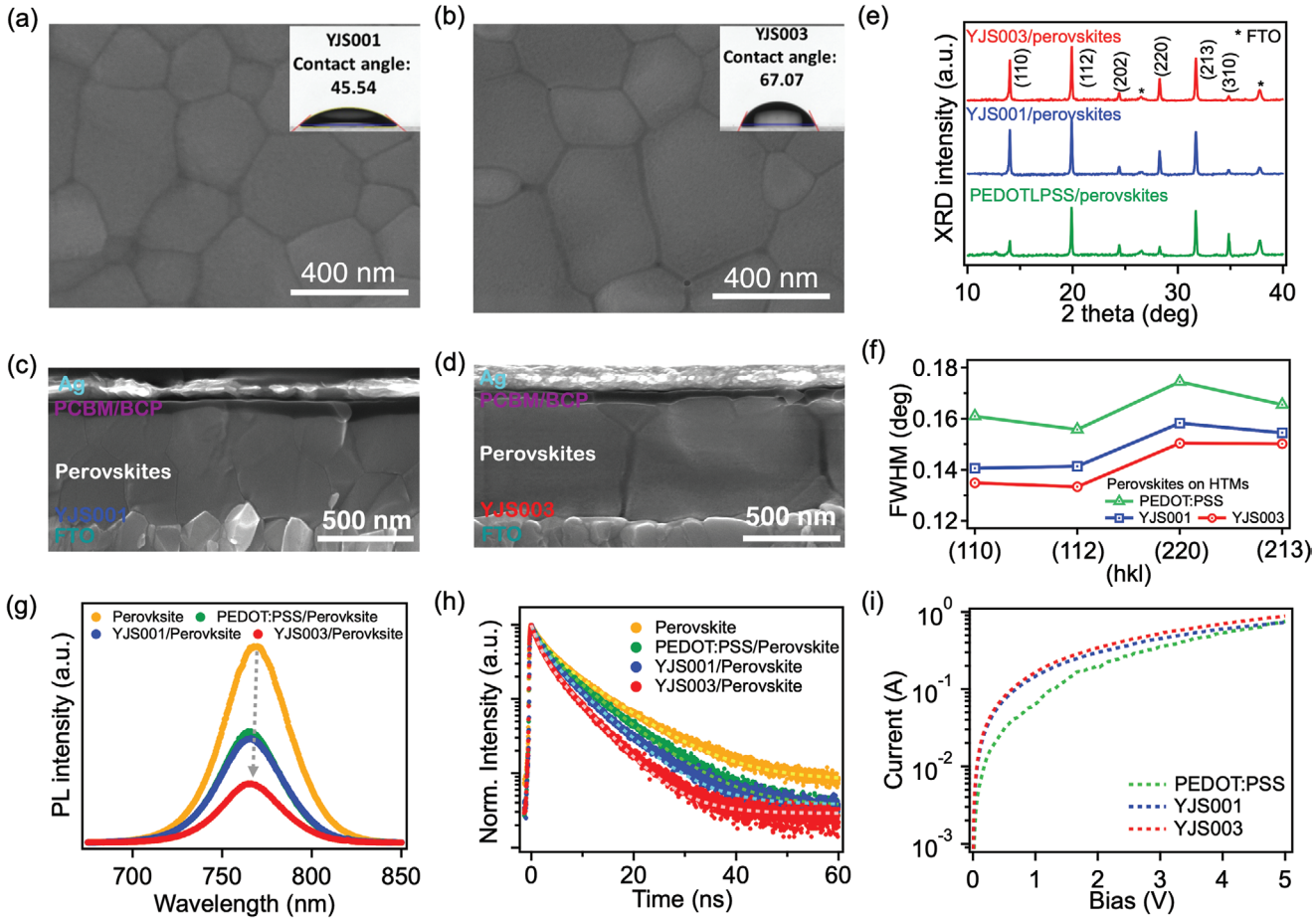

Figure 2. a,b) SEM characterizations for surface views of perovskites layers with different HTMs and c,d) cross-sectional view of perovskites devices. The inlets in the surface SEM images are the contact angles of HTMs. e) X-ray diffraction of perovskite layers on different HTMs and f) extracted FWHM of dominant peaks from (e). g) Steady-state and h) time-resolved photoluminescence for perovskites and perovskites/HTM interface. i) SCLC measurement for HTM mobility with the configuration of FTO/HTM/Au.

matches the cross-sectional SEM observations in Figures 2c,d. In addition, we utilized photoluminescence (PL) and time-resolved PL (TRPL) to study and understand the charge transfer and carrier recombination process at the perovskite/HTM interfaces (Figure 2g,h). Figure 2g compares the PL spectra of perovskite thin films on glass and on various HTMs when excited under the same laser power, where the perovskite only thin film has the highest PL intensity. Comparing the perovskite thin films, the PL intensities decrease when perovskites interface with HTMs, due to interfacial charge transfer. Interestingly, the perovskite/**YJS003** has the weakest PL intensity, whereas the perovskites on **PEDOT:PSS** and **YJS001** have comparable PL intensity. We further measured TRPL and extracted average carrier lifetime from the decay curve. The average decay time (τ) for perovskite-only, perovskite/**YJS001**, and perovskite/**YJS003** thin films are 9.82 ns, 5.77 ns, and 0.68 ns, respectively. We note that the PL intensity and carrier lifetime depend on the thin film trap density, interfacial defects, and mismatch of energy levels.[22] From the crystalinity analysis by SEM and XRD, we believe the trap density in perovskite/**YJS0003** is minimal. Therefore, lower PL intensity and shorter lifetime are attributed to an efficient charge seperation from perovskites layer to the **YJS003**.

Furthermore, the HTMs mobility also plays a vital role in charge transfer and device physics. Therefore, we performed the space charge limited current (SCLC) measurement with the device structure of fluorine-doped tin oxide (FTO)/HTMs/Au. After fitting the SCLC curves (Figure 2i), the hole mobility of **YJS001** is 3.31×10^{-4} cm^2 v^{-1} s^{-1}, whereas the hole mobility is 3.98×10^{-4} cm^2 v^{-1} s^{-1} for **YJS003** and 3.15×10^{-4} cm^2 v^{-1} s^{-1} for **PEDOT:PSS**.

After a comprehensive material characterization for the perovskite layer coated on these HTMs, we assembled the photovoltaic devices and investigated their performance using these new HTMs. We fabricated a *p-i-n* device with device architecture of "FTO/HTM/triple-cation lead mixed-halide perovskites/[6,6]-phenyl-C_{61}-butyric acid methyl ester (PCBM)/bathocuproine (BCP)/Ag" (**Figure 3**a). Here, we used commonly studied triple-cation lead mixed-halide perovskites ($Cs_{0.05}FA_{0.78}MA_{0.17}PbI_{2.53}Br_{0.47}$, depict FAMACs) as the photoactive absorber and PCBM as electron transporting material (ETM). The HTMs and PCBM/BCP layers were coated by the spin-cast method, and the Ag electrode deposited was prepared using thermal evaporation with a shadow mask to define the working area. The energy level diagram for each component used in the device is

© 2022 National Central University/National Taipei University of Technology.
Advanced Functional Materials published by Wiley-VCH GmbH

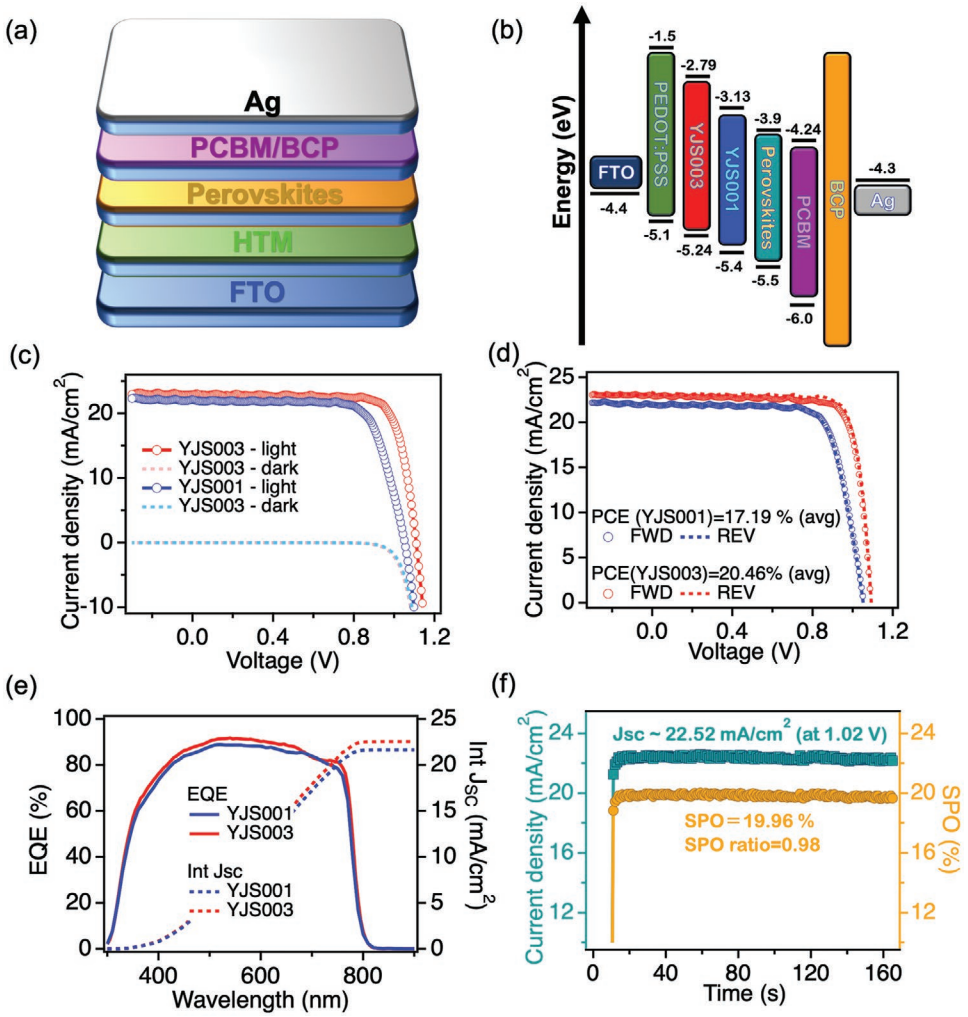

Figure 3. a) Schematic representation of planar *p-i-n* PSC device geometry and b) their corresponding energy diagrams utilized in this study. c) *J-V* characteristic curves under dark and illumination conditions with HTMs and d) the corresponding device hysteresis behavior test. e) EQE spectra of devices from (c) and the integrated J_{SC} obtained from EQE. f) Stabilized photocurrent measurement and power output of the best device using **YJS003** as HTM at the maximum power point (1.02 V).

compared and shown in Figure 3b. The energy levels (HOMO/LUMO) of **YJS001** and **YJS003** are obtained by absorption and electrochemistry from Table 1. From the energy level diagram, **YJS001** and **YJS003** have much deeper HOMO than **PEDOT:PSS** due to the central benzimidazole moiety. A deeper HOMO has been recognized as one of the key factors to achieve the high V_{OC} of the solar cell.[23] We then fabricated the photoactive layer of triple-cation lead mixed-halide perovskites onto these HTMs (please see experimental details), resulting in comparable film thickness (≈600 nm) as shown by cross-sectional SEM images in Figures 2c,d. Figure 3c exhibits the current density–voltage (*J–V*) characteristic curves for the solar cell under dark and light conditions, and the corresponding device statistics are summarized in **Table 2** by averaging over 50 cells. Both dark *J–V* curves exhibit classical diodes behavior and have strong responses under illumination. The photovoltaic devices using **YJS003** and **YJS003** outperformed the **PEDOT:PSS**-based device (Figure S4, Supporting Information). For **YJS001** and **YJS003**, the V_{OC} (1.092 V) and short-circuit current density (J_{SC}) (23.12 mA cm^{-2}) in **YJS003** cells are higher than those in **YJS001** devices (V_{OC} = 1.053 V and J_{SC} = 22.05 mA cm^{-2}), which is mainly attributed to the better energy alignment in **YJS003** with perovskites. We also examined the device hysteresis behavior (Figure 3d) to evaluate the reliability of the performance, which is heavily

Table 2. The best efficiency performances of the PSCs based on various HTMs.

HTM	V_{OC} [V]	J_{SC} [mA cm^2]	*FF*	η [%]	
				Average	Champion
PEDOT:PSS (Forward)	0.885	19.96	76.42	13.01	13.50
PEDOT:PSS (Reverse)	0.886	20.17	76.71	13.42	13.71
YJS001 (Forward)	1.052	21.97	73.63	16.94	17.02
YJS001 (Reverse)	1.054	22.13	74.42	17.23	17.36
YJS003 (Forward)	1.091	22.94	80.35	19.86	20.11
YJS003 (Reverse)	1.093	23.29	81.74	20.46	20.81

Note: FF = fill factor; η = PSC efficiency.

© 2022 National Central University/National Taipei University of Technology. Advanced Functional Materials published by Wiley-VCH GmbH

correlated to photoactive material quality and interfaces with the HTM and ETM. From the *J–V* scan in Figure 3d, both **YJS001**- and **YJS003**-based devices exhibit well overlapping forward and reverse scans, which is indicative of negligible hysteresis. The average PCEs for **YJS001** and **YJS003** are 17.09% and 20.16%, with the champion PCE of 17.36% and 20.81%, respectively. The external quantum efficiency (EQE) for these devices are shown in Figure 3e, as well as integrated photocurrent from their corresponding EQE. The **YJS003** devices have higher EQE than those of **YJS001** cells over the entire wavelength range. As a result, the integrated photocurrents are 21.67 mA cm^{-2} and 22.56 mA cm^{-2} for **YJS001** and **YJS003**, respectively, comparable to the current density obtained from experimental *J–V* measurement with less than 3% difference. To gain a better understanding of the device behavior of champion photovoltaic cells (**YJS003**), we performed the stabilized power output (SPO) by measuring the current density under a fixed maximum power point (MPP) voltage.[24] As shown in Figure 3f, the current density (22.52 mA cm^{-2}) and efficiency (19.96%) of the device reach stabilized value within 1 s under constant operation at the MPP voltage condition. The SPO-to-PCE (SPO ratio) is the difference between efficiency collected from *J–V* measurement and stabilized power output. The SPO ratio of our champion device is 0.98, which implies the low trap-density for trap-assist recombination in perovskite thin film.[24b,25] Figure S5 (Supporting Information) depicts the results of device stability investigations used to evaluate the practical application of **YJS-**HTMs based PSCs. Over 300 h continue operation under one-sun intensity, devices fabricated with **YJS001**, **YJS003**, and **PEDOT:PSS** as HTMs retained 67%, 88%, and 72% of their original PCE, respectively. These findings suggest that the **YJS003** HTM is ideal for achieving stable PSC.

To gain further insight into the charge recombination mechanism during solar cell operation using these HTMs, we investigated the illumination intensity dependencies in **Figure 4**. Figure 4a,b shows the *J–V* characteristic curves of perovskite devices with **YJS001** and **YJS003** under varying light intensity from 1-Sun (100 mW cm^{-2}) to 0.1-Sun (10 mW cm^{-2}). Figure 4c is the linear fit of V_{OC} versus the logarithm of light intensity. A slope of 1.19 kT q^{-1} is fitted for the **YJS001** device whereas the slope is 1.15 kT/q for **YJS003** devices. If the device is free from trap assisted recombination, the slope should be 1 kT/q; the slope will be higher than 1 kT/q if significant traps are present. Both devices show slopes that are closer to the trap-free case, while a small deviation from the ideal case exists, suggesting that trap-assisted recombination is still present in these devices.[23a,26] Figure 4d shows photocurrents dependence on the light intensity in a logarithm–logarithm scale. By fitting the experimental data with a power law relation, power parameters of 0.78 for **YJS001** and 0.96 for **YJS003**, respectively, were obtained. When the J_{SC}-light intensity is close to linear dependence (power = 1), the free carrier can be efficiently extracted without space charge accumulation. Clearly, the light intensity study indicates that **YJS003** devices have a better linear dependence, resulting in a good charge extraction efficiency with better device performance than **YJS001** devices, as shown in Figure 3. We also perform the electrochemical impedance spectroscopy (EIS) measurement on these HTMs materials (**YJS003**, **YJS001** and **PEDOT:PSS**) in Figure S6 (Supporting Information). EIS measurement is measured on fully stacked *p-i-n* devices, the AC field frequency varies from 1 MHz–1 Hz under one-sun light intensity for probing carrier transport process and interface resistance. The EIS demonstrated two clear semi-circle at a

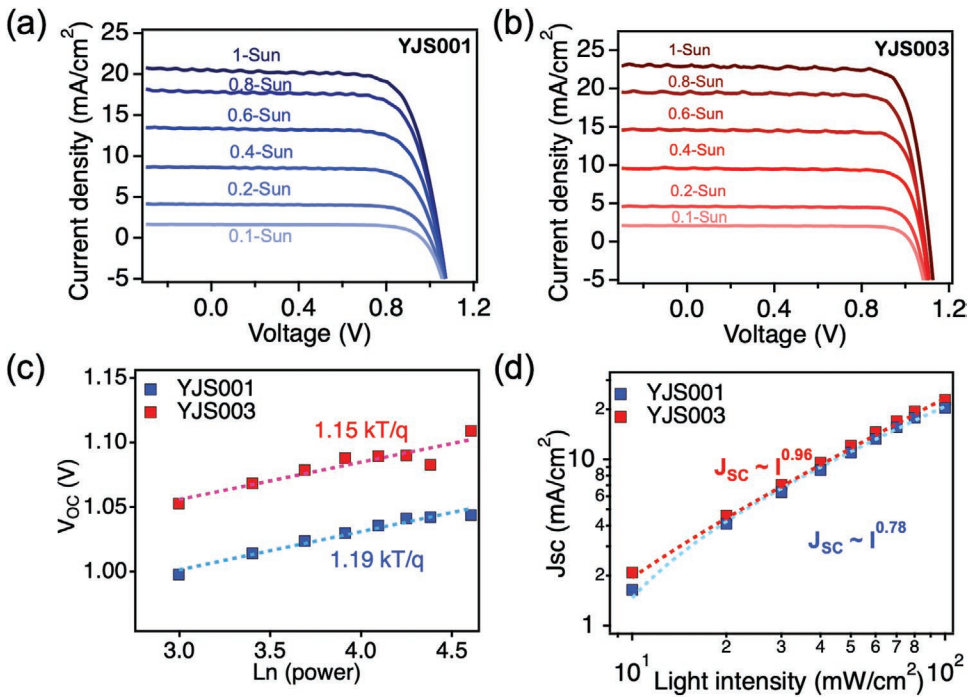

Figure 4. *J–V* characteristic curves of various light intensity for a) **YJS001** and b) **YJS003**. The c) V_{OC} and d) J_{SC} as function of light intensity of the perovskite layer growth on top of different HTMs.

© 2022 National Central University/National Taipei University of Technology. Advanced Functional Materials published by Wiley-VCH GmbH

high frequency and a lower frequency for all devices. According to the literature,[27] the high-frequency semi-circle corresponds to the charge transport resistance at HTM/perovskite interface and low-frequency semi-circle represents the interface recombination. In EIS data, the **YJS003** device exhibits lower charge transport resistance compared to other two HTM devices, which represents a better hole extraction process for the device. Besides, **YJS003** device has higher interface recombination and the low-frequency semi-circle that suggest less recombination happen in the **YJS003**/perovskites interface. The EIS data were also confirmed with the charge recombination results from light intensity measurement.

3. Conclusion

In conclusion, we demonstrated a feasible approach to energy level engineering on two new benzimidazole-based HTMs, **YJS001** and **YJS003**, by varying the donor–acceptor substituents. From the two newly synthesized and well-characterized HTMs, the photovoltaics device fabricated with the donor-rich HTM **YJS003** had better material crystallinity and PCE than **YJS001**. The enhanced performance of **YJS003** is attributed to increased $V_{OC,}$ J_{SC}, and *FF* due to good hole transport and lower series resistance, which comes from well-matched energy levels and the improvement of the perovskite/HTM interface. The improved perovskite/HTM interface can further suppress the charge recombination, resulting in high open-circuit voltage and better operation stability. These findings help shed light on the molecular-structure design and the importance of energy level engineering in HTMs toward achieving high-performance PSCs.

Supporting Information

Supporting Information is available from the Wiley Online Library or from the author.

Acknowledgements

Y.S.T., C.-C.S., Y.-C.H., J.-H.L., H.-J.L., Y.-C.H., M.-C.L., H.-H.T., Y.-H.Y., W.-Y.N., and W.-R.L. thank the Ministry of Science and Technology, ROC, for financial support (grants MOST 108-2113-M-027-002-MY, MOST 107-2113-M-027-004, and MOST 106-2113-M-008-007). This work was performed, in part, at the Center for Integrated Nanotechnologies, an Office of Science User Facility operated for the U.S. Department of Energy (DOE) Office of Science by Los Alamos National Laboratory (LANL) (Contract 89233218CNA000001).

Conflict of Interest

The authors declare no conflict of interest.

Data Availability Statement

The data that support the findings of this study are available from the corresponding author upon reasonable request.

Keywords

benzimidazole, dopant-free hole transport materials, hole mobility, inverted perovskite solar cells, perovskite absorbers

Received: February 17, 2022
Revised: May 13, 2022
Published online:

[1] a) H. Min, D. Y. Lee, J. Kim, G. Kim, K. S. Lee, J. Kim, M. J. Paik, Y. K. Kim, K. S. Kim, M. G. Kim, T. J. Shin, S. Il Seok, *Nature* **2021**, *598*, 444; b) G. Kim, H. Min, K. S. Lee, D. Y. Lee, S. M. Yoon, S. I. Seok, *Science* **2020**, *370*, 108; c) J. J. Yoo, G. Seo, M. R. Chua, T. G. Park, Y. Lu, F. Rotermund, Y.-K. Kim, C. S. Moon, N. J. Jeon, J.-P. Correa-Baena, V. Bulović, S. S. Shin, M. G. Bawendi, J. Seo, *Nature* **2021**, *590*, 587.

[2] a) L. N. Quan, B. P. Rand, R. H. Friend, S. G. Mhaisalkar, T.-W. Lee, E. H. Sargent, *Chem. Rev.* **2019**, *119*, 7444; b) W. Zhou, Z. Wen, P. Gao, *Adv. Energy Mater.* **2018**, *8*, 1702512; c) X. Yang, H. Wang, B. Cai, Z. Yu, L. Sun, *J. Energy Chem* **2018**, *27*, 650; d) H. J. Snaith, *Nature Mater* **2018**, *17*, 372; e) Y. Rong, Y. Hu, A. Mei, H. Tan, M. I. Saidaminov, S. I. Seok, M. D. McGehee, E. H. Sargent, H. Han, *Science* **2018**, *361*, 8235; f) P. Agarwala, D. Kabra, *J. Mater. Chem. A* **2017**, *5*, 1348; g) C. Wehrenfennig, G. E. Eperon, M. B. Johnston, H. J. Snaith, L. M. Herz, *Adv. Mater.* **2014**, *26*, 1584; h) G. Eperon, V. Burlakov, P. Docampo, A. Goriely, H. Snaith, *Adv. Funct. Mater.* **2014**, *24*, 151; i) S. D. Stranks, G. E. Eperon, G. Grancini, C. Menelaou, M. J. P. Alcocer, T. Leijtens, L. M. Herz, A. Petrozza, H. J. Snaith, *Science* **2013**, *342*, 341; j) J. H. Noh, S. H. Im, J. H. Heo, T. N. Mandal, S. I. Seok, *Nano Lett.* **2013**, *13*, 1764; k) J. H. Heo, S. H. Im, J. H. Noh, T. N. Mandal, C.-S. Lim, J. A. Chang, Y. H. Lee, H.-j. Kim, A. Sarkar, M. K. Nazeeruddin, M. Grätzel, S. I. Seok, *Nature Photon* **2013**, *7*, 486.

[3] a) A. Kojima, K. Teshima, Y. Shirai, T. Miyasaka, *J. Am. Chem. Soc.* **2009**, *131*, 6050; b) T. C. Sum, N. Mathews, *Energy Environ. Sci.* **2014**, *7*, 2518; c) N.-G. Park, *J. Phys. Chem. Lett.* **2013**, *4*, 2423; d) H. Zhou, Q. Chen, G. Li, S. Luo, T.-b. Song, H.-S. Duan, Z. Hong, J. You, Y. Liu, Y. Yang, *Science* **2014**, *345*, 542; e) H. J. Snaith, *J. Phys. Chem. Lett.* **2013**, *4*, 3623; f) Y. Wang, W. Chen, L. Wang, B. Tu, T. Chen, B. Liu, K. Yang, C. W. Koh, X. Zhang, H. Sun, G. Chen, X. Feng, H. Y. Woo, A. B. Djurišić, Z. He, X. Guo, *Adv. Mater.* **2019**, *31*, 1902781.

[4] a) H. D. Pham, L. Xianqiang, W. Li, S. Manzhos, A. K. K. Kyaw, P. Sonar, *Energy Environ. Sci.* **2019**, *12*, 1177; b) Y. Xia, C. Ran, Y. Chen, Q. Li, N. Jiang, C. Li, Y. Pan, T. Li, J. Wang, W. Huang, *J. Mater. Chem. A* **2017**, *5*, 3193; c) L. Meng, J. You, T.-F. Guo, Y. Yang, *Acc. Chem. Res.* **2016**, *49*, 155; d) J. H. Heo, H. J. Han, D. Kim, T. K. Ahn, S. H. Im, *Energy Environ. Sci.* **2015**, *8*, 1602.

[5] a) H. Cho, Y.-H. Kim, C. Wolf, H.-D. Lee, T.-W. Lee, *Adv. Mater.* **2018**, *30*, 1704587; b) Z. Xiao, W. Meng, J. Wang, D. B. Mitzi, Y. Yan, *Mater. Horiz.* **2017**, *4*, 206.

[6] a) Y. Wang, Y. Yue, X. Yang, L. Han, *Adv. Energy Mater.* **2018**, *8*, 1800249; b) W. S. Yang, J. H. Noh, N. J. Jeon, Y. C. Kim, S. Ryu, J. Seo, S. I. Seok, *Science* **2015**, *348*, 1234.

[7] a) M. Pandey, G. Kapil, K. Sakamoto, D. Hirotani, M. A. Kamrudin, Z. Wang, K. Hamada, D. Nomura, H.-G. Kang, H. Nagayoshi, M. Nakamura, M. Hayashi, T. Nomura, S. Hayase, *Sustain. Energy Fuels* **2019**, *3*, 1739; b) Y. Li, W. Sun, F. Gu, D. Ouyang, Z. Bian, Z. Liu, W. C. H. Choy, T. L. Kelly, *Adv. Mater. Interfaces* **2019**, *6*, 1900474.

[8] a) Z. H. Bakr, Q. Wali, A. Fakharuddin, L. Schmidt-Mende, T. M. Brown, R. Jose, *Nano Energy* **2017**, *34*, 271; b) L. Calió,

© 2022 National Central University/National Taipei University of Technology. Advanced Functional Materials published by Wiley-VCH GmbH

S. Kazim, M. Grätzel, S. Ahmad, *Angew. Chem., Int. Ed.* **2016**, *55*, 14522; c) Z. Yu, L. Sun, *Adv. Energy Mater.* **2015**, *5*, 1500213.

[9] a) Z. Shi, A. Jayatissa, *Materials* **2018**, *11*, 729; b) J. Burschka, N. Pellet, S.-J. Moon, R. Humphry-Baker, P. Gao, M. K. Nazeeruddin, M. Grätzel, *Nature* **2013**, *499*, 316.

[10] A. A. Said, J. Xie, Q. Zhang, *Small* **2019**, *15*, 1900854.

[11] a) K. Sun, S. Zhang, P. Li, Y. Xia, X. Zhang, D. Du, Isikgor, F. H.; , J. Ouyang, *J. Mater. Sci.: Mater. Electron.* **2015**, *26*, 4438; b) L. Groenendaal, F. Jonas, D. Freitag, H. Pielartzik, J. R. Reynolds, *Adv. Mater.* **2000**, *12*, 481.

[12] a) Y. Fang, X. Wang, Q. Wang, J. Huang, T. Wu, *Phys. Status Solidi A* **2014**, *211*, 2809; b) J. Yang, B. D. Siempelkamp, D. Liu, T. L. Kelly, *ACS Nano* **2015**, *9*, 1955.

[13] a) K. Rakstys, C. Igci, M. K. Nazeeruddin, *Chem. Sci.* **2019**, *10*, 6748; b) C. Rodríguez-Seco, L. Cabau, A. Vidal-Ferran, E. Palomares, *Acc. Chem. Res.* **2018**, *51*, 869; c) Z. Deng, S. Cui, K. Kou, D. Liang, X. Shi, J. Liu, *Front. Chem.* **2021**, *9*, 664504; d) G.-W. Kim, H. Choi, M. Kim, J. Lee, S. Y. Son, T. Park, *Adv. Energy Mater.* **2020**, *10*, 1903403; e) H. D. Pham, T. C.-J. Yang, S. M. Jain, G. J. Wilson, P. Sonar, *Adv. Energy Mater.* **2020**, *10*, 1903326.

[14] a) M. M. H. Desoky, M. Bonomo, R. Buscaino, A. Fin, G. Viscardi, C. Barolo, P. Quagliotto, *Energies* **2021**, *14*, 2279; b) L. Duan, Y. Chen, J. Yuan, X. Zong, Z. Sun, Q. Wu, S. Xue, *Dyes Pigm.* **2020**, *178*, 108334; c) Y.-C. Chen, D.-Z. Lin, J.-C. Wang, J.-S. Ni, Y.-Y. Yu, C.-P. Chen, *Mater. Chem. Front.* **2021**, *5*, 1373; d) E. Sheibani, L. Yang, J. Zhang, *Sol. RRL* **2020**, *4*, 2000461.

[15] a) L. Duan, Y. Chen, J. Jia, X. Zong, Z. Sun, Q. Wu, S. Xue, *ACS Appl. Energy Mater.* **2020**, *3*, 1672; b) Y. Lin, L. Shen, J. Dai, Y. Deng, Y. Wu, Y. Bai, X. Zheng, J. Wang, Y. Fang, H. Wei, W. Ma, X. C. Zeng, X. Zhan, J. Huang, *Adv. Mater.* **2017**, *29*, 1604545; c) K. Jiang, J. Wang, F. Wu, Q. Xue, Q. Yao, J. Zhang, Y. Chen, G. Zhang, Z. Zhu, H. Yan, L. Zhu, H.-L. Yip, *Adv. Mater.* **2020**, *32*, 1908011; d) R. Shang, Z. Zhou, H. Nishioka, H. Halim, S. Furukawa, I. Takei, N. Ninomiya, E. Nakamura, *J. Am. Chem. Soc.* **2018**, *140*, 5018; e) A. Magomedov, A. Al-Ashouri, E. Kasparavičius, S. Strazdaite, G. Niaura, M. Jošt, T. Malinauskas, S. Albrecht, V. Getautis, *Adv. Energy Mater.* **2018**, *8*, 1801892; f) S. B. Akula, C. Su, Y.-T. Wang, Y. S. Tingare, B.-R. Chen, Y.-C. Jheng, Y.-J. Lin, H.-C. Lan, Y.-C. Chang, W. Lekphet, W.-R. Li, *J. Power Sources* **2021**, *483*, 229177; g) W. Chen, Y. Wang, G. Pang, C. W. Koh, A. B. Djurišić, Y. Wu, B. Tu, F.-z. Liu, R. Chen, H. Y. Woo, X. Guo, Z. He, *Adv. Funct. Mater.* **2019**, *29*, 1808855.

[16] a) F. Wu, Y. Ji, C. Zhong, Y. Liu, L. Tan, L. Zhu, *Chem. Commun.* **2017**, *53*, 8719; b) G. Wu, Y. Zhang, R. Kaneko, Y. Kojima, Q. Shen, A. Islam, K. Sugawa, J. Otsuki, *J. Phys. Chem. C* **2017**, *121*, 17617; c) P. Xu, P. Liu, Y. Li, B. Xu, L. Kloo, L. Sun, Y. Hua, *ACS Appl. Mater. Interfaces* **2018**, *10*, 19697.

[17] a) S. Riera-Galindo, A. Orbelli Biroli, A. Forni, Y. Puttisong, F. Tessore, M. Pizzotti, E. Pavlopoulou, E. Solano, S. Wang, G. Wang, T.-P. Ruoko, W. M. Chen, M. Kemerink, M. Berggren, G. di Carlo, S. Fabiano, *ACS Appl. Mater. Interfaces* **2019**, *11*, 37981; b) E. Horak, R. Vianello, I. Steinberg, in *Benzimidazole and its Derivatives*, (Ed: M. Marinescu), IntechOpen, London, UK **2019**.

[18] a) X. Li, M. Ibrahim Dar, C. Yi, J. Luo, M. Tschumi, S. M. Zakeeruddin, M. K. Nazeeruddin, H. Han, M. Grätzel, *Nat. Chem.* **2015**, *7*, 703; b) K. Zhu, S. Cong, Z. Lu, Y. Lou, L. He, J. Li, J. Ding, N. Yuang, M. H. Rümmeli, G. Zou, *J. Power Sources* **2019**, *428*, 82.

[19] R. Wang, S. V. Ranganathan, P. Haruehanroengra, S. Mao, M. Scalabrin, D. Fabris, A. Chen, H. Liu, A. E. A. Hassan, J. Gan, J. Sheng, *J. Biomol. Struct. Dyn.* **2019**, *37*, 551.

[20] a) Y. Gao, Y. Wu, Y. Liu, M. Lu, L. Yang, Y. Wang, W. W. Yu, X. Bai, Y. Zhang, Q. Dai, *Nanoscale Horiz.* **2020**, *5*, 1574; b) H. Li, G. Wu, W. Li, Y. Zhang, Z. Liu, D. Wang, S. Liu, *Adv. Sci.* **2019**, *6*, 1901241; c) C. Bi, Q. Wang, Y. Shao, Y. Yuan, Z. Xiao, J. Huang, *Nat. Commun.* **2015**, *6*, 7747.

[21] a) H.-H. Huang, H. Tsai, R. Raja, S.-L. Lin, D. Ghosh, C.-H. Hou, J.-J. Shyue, S. Tretiak, W. Chen, K.-F. Lin, W. Nie, L. Wang, *ACS Energy Lett.* **2021**, *6*, 3376; b) M. Saliba, T. Matsui, J.-Y. Seo, K. Domanski, J.-P. Correa-Baena, M. K. Nazeeruddin, S. M. Zakeeruddin, W. Tress, A. Abate, A. Hagfeldt, M. Grätzel, *Energy Environ. Sci.* **2016**, *9*, 1989.

[22] a) H. Tsai, C. Liu, E. Kinigstein, M. Li, S. Tretiak, M. Cotlet, X. Ma, X. Zhang, W. Nie, *Adv. Sci.* **2020**, *7*, 1903202; b) Y. Zhou, K. Fernando, J. Wan, F. Liu, S. Shrestha, J. Tisdale, C. J. Sheehan, A. C. Jones, S. Tretiak, H. Tsai, H. Huang, W. Nie, *Adv. Funct. Mater.* **2021**, *31*, 2101058; c) S. Feldmann, S. Macpherson, S. P. Senanayak, M. Abdi-Jalebi, J. P. H. Rivett, G. Nan, G. D. Tainter, T. A. S. Doherty, K. Frohna, E. Ringe, R. H. Friend, H. Sirringhaus, M. Saliba, D. Beljonne, S. D. Stranks, F. Deschler, *Nat. Photonics* **2020**, *14*, 123; d) T. Jiang, Z. Chen, X. Chen, X. Chen, X. Xu, T. Liu, L. Bai, D. Yang, D. Di, W. E. I. Sha, H. Zhu, Y. M. Yang, *ACS Energy Lett.* **2019**, *4*, 1784.

[23] a) C.-Y. Chang, H.-H. Huang, H. Tsai, S.-L. Lin, P.-H. Liu, W. Chen, F.-C. Hsu, W. Nie, Y.-F. Chen, L. Wang, *Adv. Sci.* **2021**, *8*, 2002718; b) J. D. Servaites, M. A. Ratner, T. J. Marks, *Energy Environ. Sci.* **2011**, *4*, 4410; c) C.-G. Wu, C.-H. Chiang, S. H. Chang, *Nanoscale* **2016**, *8*, 4077.

[24] a) Q. Ye, Y. Zhao, S. Mu, F. Ma, F. Gao, Z. Chu, Z. Yin, P. Gao, X. Zhang, J. You, *Adv. Mater.* **2019**, *31*, 1905143; b) Z. Wang, Q. Lin, F. P. Chmiel, N. Sakai, L. M. Herz, H. J. Snaith, *Nat. Energy* **2017**, *2*, 17135.

[25] W. Li, W. Zhang, S. Van Reenen, R. J. Sutton, J. Fan, A. A. Haghighirad, M. B. Johnston, L. Wang, H. J. Snaith, *Energy Environ. Sci.* **2016**, *9*, 490.

[26] a) S. Shao, Z. Chen, H. H. Fang, G. H. ten Brink, D. Bartesaghi, S. Adjokatse, L. J. A. Koster, B. J. Kooi, A. Facchetti, M. A. Loi, *J. Mater. Chem. A* **2016**, *4*, 2419; b) Y. Liu, Z. Hong, Q. Chen, W. Chang, H. Zhou, T.-B. Song, E. Young, Y. Yang, J. You, G. Li, Y. Yang, *Nano Lett.* **2015**, *15*, 662; c) M. M. Mandoc, F. B. Kooistra, J. C. Hummelen, B. d. Boer, P. W. M. Blom, *Appl. Phys. Lett.* **2007**, *91*, 263505.

[27] a) M.-H. Liu, Z.-J. Zhou, P.-P. Zhang, Q.-W. Tian, W.-H. Zhou, D.-X. Kou, S.-X. Wu, *Opt. Express* **2016**, *24*, A1349; b) G. Murugadoss, H. Kanda, S. Tanaka, H. Nishino, S. Ito, H. Imahori, T. Umeyama, *J. Power Sources* **2016**, *307*, 891; c) E. Nouri, M. R. Mohammadi, P. Lianos, *ACS Omega* **2018**, *3*, 46.

© 2022 National Central University/National Taipei University of Technology.
Advanced Functional Materials published by Wiley-VCH GmbH